Photoemission spectroscopy of high-T_c superconductors

E. G. Maksimov and S. Yu. Savrasov

P. N. Lebedev Physics Institute, Academy of Sciences of the USSR

Usp. Fiz. Nauk **160**, 155–176 (September 1990)

A concise review of experimental results obtained by photoemission spectroscopy of high-T_c superconductors. The authors focus mainly on the normal state electronic structure of these materials. A brief outline of the experimental and theoretical foundations of photoemission spectroscopy is also provided.

1. INTRODUCTION

Since the discovery of high-T_c metal-oxide superconductors by Bednorz and Müller in 1986, the amount of experimental and theoretical research in this field has been enormous. There have been numerous attempts to uncover the mechanism responsible for the high values of the critical temperature T_c in the new high-temperature superconductors (HTSC). The various hypotheses cover a rather wide spectrum: from the more-or-less standard descriptions based on Cooper pairing of electrons via electron-phonon or electron-electron interactions, to completely new theories invoking such concepts as resonating valence bonds or spontaneous magnetic flux states. Unfortunately, the quality of experimental data and the lack of detail in the theoretical picture make it impossible to identify a unique HTSC mechanism with any confidence.

It is important to emphasize that not only do the various research groups offer radically different descriptions of the superconducting HTSC state, but they also disagree in their understanding of the normal state at temperatures above the critical value ($T > T_c$). Moreover, it is becoming ever more apparent that the key to the HTSC problem lies precisely in the detailed understanding of the normal state of these systems and especially of their electronic structure. Indeed, a number of proposed HTSC superconductivity mechanisms depend on the existence of strongly correlated electronic systems that cannot be described by the Fermi-liquid model. A number of theoretical and experimental papers have pointed to the inapplicability of the usual band structure description to the electron spectrum of HTSC systems.

Photoemission spectroscopy is one of the most powerful techniques for determining electronic structure. It is therefore not surprising that a large number of photoemission spectroscopy investigations of HTSC materials have appeared in recent years. The purpose of this review is to present and discuss the results of photoemission experiments. The review is organized as follows: first, a brief description of photoemission spectroscopy techniques and interpretation of photoemission spectra; a summary of the results obtained by photoemission spectroscopy in HTSC systems; finally, the description of the electronic properties of these systems that follows from a comparison of experimental data with various theoretical models.

2. EXPERIMENTAL TECHNIQUES OF PHOTOEMISSION SPECTROSCOPY

Photoemission spectroscopy is based on the photoeffect discovered by Hertz as early as 1887. In this effect an incident electromagnetic wave causes electron emission from the near-surface layer of a crystal. The distribution of emitted particles contains a wealth of information on the electronic energy spectrum inside the crystal.

The standard experimental arrangement is illustrated in Fig. 1. The sample is irradiated with monoenergetic photons of a given polarization $\mathbf{P}_i$. The photons are incident on the surface at a polar angle θ_i and azimuthal angle φ_i. A spectrometer is used to detect the photoelectrons emitted at angles θ_e, φ_e with energy E and spin σ. The measured photocurrent I is a function of all these parameters:

$$I = F(E,\ \theta_e,\ \varphi_e,\ \hbar\omega,\ \mathbf{P}_i,\ \theta_i,\ \varphi_i). \tag{1}$$

The purpose of the experiment is to study the dependence of I on the various parameters.

There are two major types of photoemission spectroscopy:

(a) Measurements of the electron energy dependence of the photocurrent $I(E)$ at fixed values of $\hbar\omega$, $\mathbf{P}_i$, θ_i and φ_i.

(b) Angle resolved measurements, i.e. measurements of the dependence of I on three parameters E, θ_e, and φ_e.

The above list is far from complete. Other techniques include measurement of the photocurrent dependence on photon polarization (vector photoeffect), on electron spin (spin-polarized emission), on photon energy at a fixed value of E (spectroscopy with a fixed final state), and on energies E and $\hbar\omega$ given a constant difference $(E - \hbar\omega) = \text{const}$.

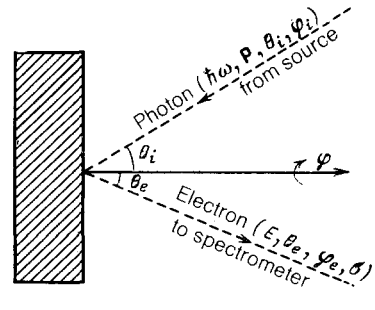

FIG. 1. Schematic photoemission experiment set-up.

 0038-5670/90/090763-12$01.00

(spectroscopy with a fixed initial state). Photoemission spectroscopy can also be subdivided according to photon energy: photoemission in the ultraviolet ($\hbar\omega < 50$ eV), soft x-ray photoemission (50 eV $< \hbar\omega < 200$ eV), and x-ray photoemission ($\hbar\omega > 200$ eV). Tunable light sources are currently available in all these spectral ranges. Usually these sources are based on synchrotron radiation from electron accelerators and characteristic x-ray frequencies.

In photoemission experiments electrons are emitted mainly from the near-surface layer that is 5–30 Å thick. The depth from which the electron is emitted depends largely on the energy of the electron, rather than on the sample material under study. Typically, electrons with energies below 10 eV or above 10 keV are emitted from a depth of the order of 20–30 Å. In the intermediate energy range, around 100 eV, the emission depth has a minimum, reaching values of only 5–10 Å. Clearly, the emission depth together with its energy dependence are of crucial importance in photoemission spectroscopy for two reasons. First, the experimental results reflect either bulk or surface properties of the sample, depending on the energy range of emitted electrons. Second, contamination or deterioration of the surface can markedly affect experimental results. Consequently, maintaining the quality of the sample surface is especially important in photoemission spectroscopy.

Until recently, energy resolution in photoemission experiments in the ultraviolet was in the 0.1–0.2 eV range. Today, a number of experimental groups have improved the energy resolution significantly, reaching the 0.01–0.02 eV range. This makes it possible to study the measured spectra in sufficient detail and observe their evolution during a superconducting transition. Energy resolution of experiments employing characteristic x-ray radiation is much lower, around ~ 1 eV. X-ray monochromators can improve this resolution to 0.5–0.6 eV, but the radiation intensity is then about three orders of magnitude lower than in the ultraviolet.

3. INTERPRETATION OF PHOTOEMISSION SPECTRA

Interpretation of photoemission spectra requires information on the behavior of electrons in the solid under the influence of a periodic potential, on the perturbations caused by the solid–vacuum interface, on electron interaction with other electrons, lattice phonons, etc., and on the photoemission mechanism set in motion by the external electromagnetic wave. Obviously, nearly all of the above problems are fundamental to solid state physics and no rigorous theoretical solutions are available. Nonetheless, the present state of solid state theory suffices not only for a qualitative, but often a quantitative description of photoemission spectra. A subsequent comparison of theoretical and experimental spectra can therefore provide information on the electronic structure of the system under study. We will not discuss rigorous many-body formulations of photoemission theory, nor will we describe the techniques by which the problem can be reduced to a simpler, single-particle description of electrons in a crystal. The interested reader is refered to the monograph of Ref. 1, where both a thorough discussion of the problem and an exhaustive bibliography are available. In this review we will restrict ourselves to the popular semi-empirical three-step model of the photoemission process.

As an example, consider the emission process of a valence electron from the crystal. At long wavelengths ($\hbar\omega < 200$ eV), the first step can be described as a direct optical transition of the electron from an occupied state in the conduction band to a higher-lying band (Fig. 2). This process conserves both energy

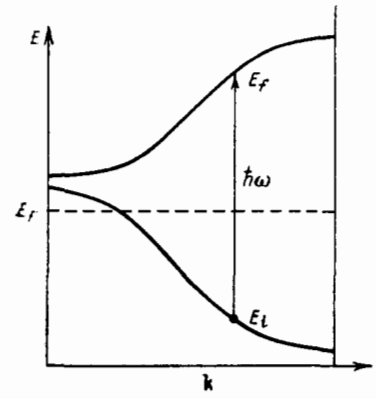

FIG. 2. Optical transition of an electron to the conduction band due to photon absorption.

$$E_f(\mathbf{k}) - E_i(\mathbf{k}) = \hbar\omega \tag{2}$$

and crystal momentum

$$\hbar\mathbf{k}_f = \hbar\mathbf{k}_i = \hbar\mathbf{K}_i - \hbar\mathbf{G}, \tag{3}$$

where $\hbar\mathbf{K}_f$ is the momentum of the excited electron in the extended band scheme and $\mathbf{G}$ is a reciprocal lattice vector. The second step consists of electron propagation to the surface, which can involve inelastic scattering from other electrons in the crystal. In the third step the electron is emitted into the vacuum–this process does not conserve the momentum component normal to the surface, $\hbar\mathbf{K}_{f\perp} \neq$ const., but it does conserve the parallel momentum component, $\hbar\mathbf{K}_{f\parallel} = \hbar\mathbf{k}_{i\parallel} + \mathbf{G}_{\parallel}$. The three-step model can be employed to interpret photoemission spectra. In this model the photoemission intensity can be divided into two terms:

$$I(E, \omega) = I_1(E, \omega) + I_2(E, \omega). \tag{4}$$

The first term describes the flux of primary electrons that leave the crystal without losing any energy. The second term describes the background of secondary electrons that lose energy via inelastic collisions. The quantity I_1 can be written as a product of three factors:

$$I_1(E, \omega) = P(E, \omega)T(E, \omega)D(E, \omega), \tag{5}$$

where $P(E,\omega)$ is the distribution of photoexcited photoelectrons; $T(E,\omega)$ is the transfer probability; $D(E,\omega)$ is the exit function. Assume that the probability of inelastic scattering can be characterized by an average isotropic mean free path $\lambda_e(E)$. Since the penetration depth of electromagnetic waves $\lambda_p(\omega)$ in metals is of the order of 100 Å, it is larger than the mean free path of electrons with energy < 100 eV ($\sim$10–30 Å) by an order magnitude. Consequently, the transfer probability is simply proportional to the ratio $\lambda_e(E)/\lambda_p(\omega)$. It is precisely the transfer probability that ultimately determines the extreme sensitivity of photoemission spectra to the quality of the surface. Only electrons from the near-surface layer 10–30 Å deep can be emitted without energy loss. Generally speaking, the band structure of the

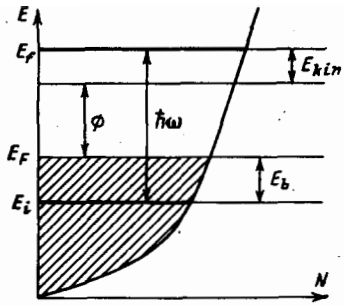

FIG. 3. Energy diagram of the photoemission process.

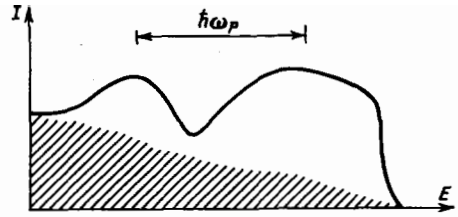

FIG. 4. Typical photoemission spectrum of a normal metal. Hatched region corresponds to the growing secondary electron background.

near-surface layer can differ from the bulk, but available experimental information indicates that the near-surface layer "recalls" the three-dimensionality of the crystal and hence the photoemission spectra reflect the electronic structure of the bulk material.

Electron emission from a solid is only possible if the electron has sufficient kinetic energy of motion normal to the surface to surmount the surface potential barrier. In the simplest case this potential barrier is taken as $E_F + \phi$, where E_F is the Fermi energy and ϕ is the work function, i.e. the minimal energy required to remove the electron from the solid (Fig. 3). For an isotropic electron distribution this condition can be written as

$$\frac{\hbar^2 k_{i\perp}^2}{2m} + \hbar\omega > E_F + \phi, \tag{6}$$

which leads to electron emission from the surface into a cone with the opening angle given by

$$\cos\theta = \left(\frac{E_F + \phi}{E}\right)^{1/2}, \tag{7}$$

where $E = E_f = E_i + \hbar\omega$. The exit function in this model can be written as follows:

$$\begin{aligned} D(E, \omega) &= \frac{1}{2} - \frac{1}{2}\left(\frac{E_F + \phi}{E}\right)^{1/2} \quad \text{if} \quad E > E_F + \phi, \\ &= 0 \qquad\qquad\qquad\qquad\quad \text{if} \quad E < E_F + \phi. \end{aligned} \tag{8}$$

From the foregoing analysis we find that both $T(E,\omega)$ and $D(E,\omega)$ vary smoothly with energy and cannot produce any features or singularities in the photoemission spectra.

Within the framework of the three-step model, the total distribution of photoexcited electrons is given by the optical transition probability from the filled band $E_i(\mathbf{k})$ to the higher-lying band $E_f(\mathbf{k})$:

$$P(E, \omega) \sim \sum_{i,f} \int d\mathbf{k} \, |\langle i\mathbf{k} | \hat{\mathbf{p}} | f\mathbf{k}\rangle|^2 \, \delta(E_f(\mathbf{k}) - E_i(\mathbf{k}) - \hbar\omega) \, \delta(E - E_f(\mathbf{k})), \tag{9}$$

where $\hat{\mathbf{p}}$ is the momentum operator and the summation runs over all occupied (i) and unoccupied (f) states. The first δ-function ensures energy conservation in the transition, while the second indicates the detection of an electron of given energy E. As for indirect transitions, involving either phonons or photons in the x-ray range, where momentum transfer is not negligible, the matrix element can be omitted, and $P(E,\omega)$ can be trivially expressed as

$$P(E, \omega) \sim N(E) N(E - \hbar\omega), \tag{10}$$

where $N(E)$ is the density of one-electron states in the crystal. Consequently we find that the photoemission spectra of the valence band is proportional to the produce of the densities of occupied and unoccupied states. In principle, given small excitation energies, $N(E)$ can give rise to features in the photoemission spectrum if the density of low-lying excited states contains van Hove singularities. Yet as energy increases, the quantity $N(E)$ clearly will approach $E^{1/2}$, the free electron density of states. Consequently, photoemission spectra can be simply interpreted in terms of the density of occupied states.

Now let us turn to the second term in expression (4), which describes the background structure of the spectrum. Propagation of high-energy electrons through the crystal leads to energy losses via various types of excitations. Dominant among these processes are electron-hole pair and plasmon excitations. Electron-hole pair excitations produce no features in the spectrum. Plasmon excitations, on the other hand, are usually well separated from the normal valence band spectrum because of the high energy of plasma oscillations.

A typical photoemission spectrum (Fig. 4) can be easily reconstructed from the above-described picture. It should contain the valence band structure with a low-energy tail due to electron-hole pair excitation, as well as a distinct satellite peak separated from the valence band by the plasmon energy $\hbar\omega_p$. The shaded region in Fig. 4 corresponds to the increasing background of secondary electrons.

Up to this point we have implicitly assumed that the detector registers electrons of energy $E = E_f$. In fact, in the detector energy is referred to the vacuum level and the measured photoelectron energy equals E_{kin} (Fig. 3). In order to reconstruct the electron binding energies E_b in the crystal (i.e. energies referred to the Fermi energy) one must determine the work function ϕ. Then $E_b = E_{kin} + \phi - \hbar\omega$. The work function can be measured by various methods. The most common technique is based on determining the threshold optical frequency at which emission is still possible. Although it appears at first that this technique should measure ϕ with sufficient accuracy, this is actually not the case. As we have already discussed, an electron must satisfy condition (6) in order to leave the crystal. Since

$$\frac{\hbar^2 k_{i\perp}^2}{2m} + \frac{\hbar^2 k_{i\parallel}^2}{2m} < E_F,$$

only electrons with $\mathbf{k}_\parallel \sim 0$ are emitted near the threshold. As a result, the total photocurrent depends quadratically on the frequency:

$$j(\omega) \sim (\hbar\omega - \phi)^2. \tag{11}$$

Consequently, the work function is usually calculated by fit-

ting experimental parameters to a function similar to (11). We should mention other methods of determining ϕ, like the contact potential difference method and thermoemission measurements.

4. ANGLE-RESOLVED PHOTOEMISSION AND ELECTRON SPECTRA OF CRYSTALS

Until now we have been discussing photoemission measurements which monitor only the energy of the emitted electrons. Such measurements make it possible to determine some average properties of occupied bands. Angle-resolved photoemission, i.e. measurement of both kinetic energy and propagation direction of the photoelectron (described by angles θ_e and φ_e, see Fig. 1), can reproduce the (almost) complete spectrum of elementary excitations, i.e. the quantity $E_i(\mathbf{k}_i)$. Indeed, angle-resolved measurements determine not only the magnitude of the momentum $\mathbf{k}_f$ of the emitted photoelectron (by virtue of $E_{kin} = \hbar \mathbf{K}_f^2/2m$), but also its direction. Further, by representing the final state as a superposition of plane waves

$$|f\mathbf{k}\rangle = \sum_{\mathbf{G}} u_{\mathbf{k}+\mathbf{G}f} \exp[i(\mathbf{k}+\mathbf{G})\mathbf{r}], \tag{12}$$

we can easily show that electron emission into the vacuum conserves the wavevector component parallel to the interface

$$\mathbf{K}_{f\parallel} = \mathbf{k}_{i\parallel} + G_{\parallel}. \tag{13}$$

Conservation of energy then immediately yields the binding energy:

$$E_b(\mathbf{k}_i) = E_i(\mathbf{k}_i) - E_F - E_{kin} + \phi - \hbar\omega. \tag{14}$$

Unfortunately, this procedure cannot yield the complete momentum $\mathbf{k}_i$ of the initial state, since the perpendicular component $\mathbf{k}_{i\perp}$ does not enter into the above expressions. The only reliable result of these measurements is the line in $\mathbf{k}$-space on which the initial electron state must lie, which is

$$\mathbf{k}_{i\parallel} = \left(\frac{2mE_{kin}}{\hbar^2}\right)^{1/2} \sin\theta - \mathbf{G}_{\parallel}. \tag{15}$$

Thus, it turns out that experiment cannot yield the full three-dimensional electronic structure directly. This is the limitation we mentioned in the beginning of this section.

There exist several methods of overcoming this problem, however. First, the results obtained by angle-resolved photoemission spectroscopy are already sufficient for comparison with theoretically computed electronic spectra. Second, in a number of special cases, experimental results can yield a complete description of the electronic spectrum, at least along some principal directions. An example of this is any layered compound which is dispersionless along one axis. Another example is the so-called normal emission technique, which monitors photoelectrons emitted normal to the sample surface. Since $\mathbf{k}_{\parallel} = 0$, this technique is limited to a single line through the Brillouin zone. Assuming the dispersion of the final state can be written as

$$\frac{\hbar^2 \mathbf{k}_{i\perp}^2}{2m} = E_{kin} + \phi + E_F, \tag{16}$$

we can solve for the wavevector component normal to the sample surface.

Normal emission experiments are quite attractive since they measure the band structure along a direction of high symmetry for which $\mathbf{k}_{\parallel} = 0$. This technique can be generalized and applied to other directions by fixing a constant final state. The electron energy analyzer is set for fixed values of E_{kin}, θ_e, and φ_e, which gives $\mathbf{k}_{\parallel} = \text{const}$. Then, by varying the photon frequency we can scan along the $\mathbf{k}_{\parallel} = \text{const}$. direction through the Brillouin zone. The unknown quantity $\mathbf{k}_{i\perp}$ can also be calculated from the equality

$$\frac{\hbar^2 \mathbf{k}_{i\perp}^2}{2m} + \frac{\hbar^2 \mathbf{k}_{i\parallel}^2}{2m} = E_{kin} + \phi + E_F \tag{17}$$

Now consider the important problem of the angular resolution of the spectrometer. Since the quantity $\mathbf{k}_{\parallel}$ is determined by expression (15), we can estimate the uncertainty $\Delta\mathbf{k}_{\parallel}$ in the parallel component of the wavevector for $\Delta\theta = 4°$, $\theta = 45°$, and $E = 15$ eV to be ≈ 0.1 Å, i.e. approximately 0.1 of the size of the Brillouin zone. On the other hand, if the energy is of the order of 1500 eV, we find $\Delta\mathbf{k}_{\parallel} \approx 1$ Å, i.e. of the same order as the size of the Brillouin zone. Hence photon energies in the ultraviolet are essential for reliable band structure investigations.

The above interpretation of photoemission measurements assumes that the solid contains stable single-electron states. These states are generally constructed by the density functional method.[2] Within the framework of this method one can show that the energy of a system in an external field is a single-valued density function that can be written in the following form:

$$E_{tot}\{\rho\} = T_0\{\rho\} + \int V_{ion}(\mathbf{r})\rho(\mathbf{r})\,d\mathbf{r} + \frac{e^2}{2}\iint \frac{\rho(\mathbf{r})\rho(\mathbf{r}')}{|\mathbf{r}-\mathbf{r}'|}\,d\mathbf{r}\,d\mathbf{r}' + E_{xc}\{\rho\}; \tag{18}$$

where $T_0(\rho)$ is the kinetic energy of an inhomogeneous system of noninteracting electrons with the same density ρ and E_{xc} is the exchange correlation energy. The true density distribution corresponds to the minimum of the functional

$$\frac{\delta E_{tot}\{\rho\}}{\delta\rho} = 0. \tag{19}$$

Writing the density as

$$\rho(\mathbf{r}) = \sum_i^{occ} |\psi_i(\mathbf{r})|^2, \tag{20}$$

we can obtain a Schrödinger-type equation for the functions Ψ_i

$$\left(-\frac{\hbar^2\nabla^2}{2m} + V_{eff}(\mathbf{r})\right)\psi_i(\mathbf{r}) = E_i\psi_i(\mathbf{r}), \tag{21}$$

where

$$V_{eff}(\mathbf{r}) = V_{ion}(\mathbf{r}) + e^2\int \frac{\rho(\mathbf{r}')}{|\mathbf{r}-\mathbf{r}'|}\,d\mathbf{r}' + V_{xc}(\mathbf{r}), \tag{22}$$

and

$$V_{xc}(\mathbf{r}) = \frac{\delta E_{xc}\{\rho\}}{\delta\rho(\mathbf{r})}. \tag{23}$$

By using a local density approximation for the exchange correlation energy

$$E_{xc}\{\rho\} = \int \varepsilon_{xc}\{\rho(\mathbf{r})\}\rho(\mathbf{r})\,d\mathbf{r} \tag{24}$$

or some more sophisticated approximation, we obtain a self-consistent set of equations (20)–(24) for the total energy of electrons in the crystal. the resulting set of single-particle states E_i comprises the usual definition of band structure. This is the model considered in most studies comparing experimental and theoretical photoemission spectra. We should emphasize at once that by virtue of their derivation in the density functional framework, the eigenfunctions E_i of the Kohn–Sham equations (21) do not represent the true single-particle electronic excitation spectrum of the system, but rather provide the necessary intermediate step. The actual spectrum is determined by the poles of the single-particle Green's function; it is described by the following equation:

$$\left(-\frac{\hbar^2\nabla^2}{2m}+V_{\text{ion}}(\mathbf{r})+e^2\int\frac{\rho(\mathbf{r}')}{|\mathbf{r}-\mathbf{r}'|}\,d\mathbf{r}'\right)\tilde{\psi}_i(\mathbf{r})$$
$$+\int\Sigma_{\text{xc}}(\mathbf{r},\mathbf{r}',\tilde{E}_i)\,\tilde{\psi}_i(\mathbf{r}')\,d\mathbf{r}'=\tilde{E}_i\tilde{\psi}_i(\mathbf{r}). \qquad (25)$$

By comparing expressions (21) and (25), we find that in (25) the local exchange correlation potential V_{xc} of the Kohn–Sham equation has been replaced by the nonlocal, energy-dependent operator $\Sigma_{\text{xc}}(\mathbf{r},\mathbf{r}',\tilde{E}_i)$. The nonlocality and energy dependence of this operator can cause the single-particle excitation spectrum $\tilde{E}_i$ to differ markedly from the E_i spectrum that reflects the ground state properties. In particular, the energy dependence of $\Sigma_{\text{xc}}(\mathbf{r},\mathbf{r}',\tilde{E}_i)$ makes the eigenfunctions complex, $\tilde{E}_i=\varepsilon_i+i\Gamma_i$, and causes the lifetime of electron states to become finite, $\hbar/\tau_i=\Gamma_i$. Fortunately, both theoretical estimates and experimental results, particularly in angle-resolved photoemission spectroscopy, indicate that in most real metallic systems the difference between E_i and $\tilde{E}_i$ is sufficiently small. Figure 5 compares the theoretical spectra $E_i(\mathbf{k})$ of copper calculated by solving self-consistently the Kohn–Sham equations using the local approximation for exchange correlation energy with experimental results obtained by angle-resolved photoemission measurements. A detailed discussion of the relative unimportance of dynamical electron-electron interactions to the difference between E_i and $\tilde{E}_i$ spectra goes far beyond the scope of this review and will be omitted. It suffices to note that the broadening of photoemission spectra due to finite electron state lifetimes τ_i as well as a number of other discrepancies between E_i and $\tilde{E}_i$ spectra can be quite simply understood and evaluated by applying perturbation theory methods to the initial E_i spectrum obtained from the Kohn–Sham equations. We shall return to this problem later, when we discuss photoemission spectra of high-temperature superconductors.

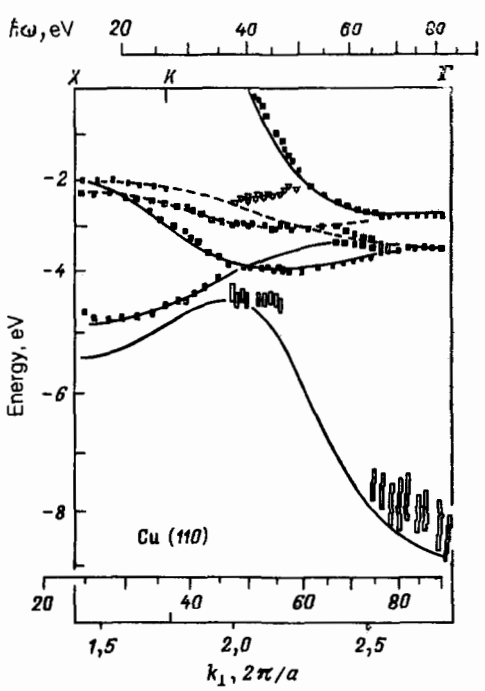

FIG. 5. Experimental valence band structure of copper. Solid lines correspond to calculations of Ref. 26; points are experimental data of Ref. 27.

5. PHOTOEMISSION EXPERIMENTS IN HTSC

Most of the photoemission results obtained in the early stages of HTSC research turned out to disagree with the calculated band structures (see Wendin's review of early experiments[3]). The discrepancies arose from the following experimental facts. First, the valence band appeared shifted towards higher binding energies by 2 eV. Second, photoemission spectra exhibited complex satellite structure beyond the valence band edge that could not be attributed to energy loss processes involving plasmon emission. Third, angle-resolved photoemission measurements indicated that the electronic excitation spectra contained no energy bands with any discernible dispersion [that is, a dependence of energy $E_i(\mathbf{k})$ on wavevector $\mathbf{k}$]. Finally and most importantly, the measured photoemission spectra contained no clear Fermi absorption edge. Since a photoemission spectrum follows the density of occupied states, in ordinary metals there should be a sharp edge at the energy corresponding to electron emission from the Fermi surface. Yet the initial photoemission curves exhibited no such edge in the vicinity of E_F, as shown in Fig. 6. This figure also plots the expected Fermi step broadened by temperature, interactions, and the finite resolution of the spectrometer. This discrepancy stimulated the appearance of a profusion of theoretical models (different variants of the Hubbard model,[4,5] resonating valence bond models[6]) based on strong electron correlations. These models predicted no Fermi-liquid-like behavior of the electronic structure.

The situation changed drastically with the discovery of

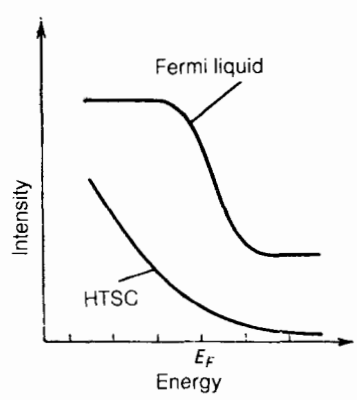

FIG. 6. Photoemission spectrum near the Fermi level observed in early experiments compared with the Fermi step expected in a normal metal.

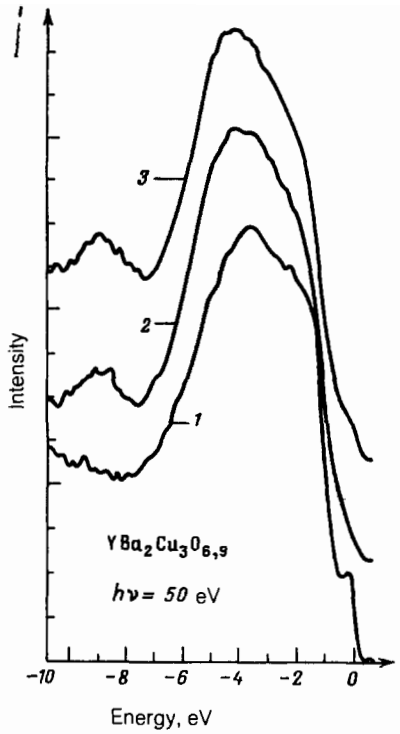

FIG. 7. Photoemission spectra of $YBa_2Cu_3O_{6.9}$ valence bands.[9] The sample was cleaved at 20 K. Curve *1* was measured immediately after cleaving; *2*–after 10 min. at 300 K; *3*–after cooling back down to 20 K.

bismuth cuprates. The first experimental confirmation of the Fermi edge was demonstrated in the $Bi_2Sr_2CaCu_2O_8$ compound[7]. Then Arco and co-workers[8] demonstrated that most room temperature photoemission spectra of 1:2:3 compounds may reflect not the bulk band structure, but rather the state of the surface. Because of the rapid evolution of oxygen from the surface, the surface electronic structure is actually closer to the antiferromagnetic state induced by the shortage of oxygen.

At present this problem has been studied in adequate detail and it has been concluded that the Fermi edge is as sharp in high-temperature superconductors as in ordinary metals. This is illustrated in the results of Arco and co-workers[9] who measured the valence band of $YBa_2Cu_3O_{6.9}$ at $\hbar\omega = 50$ eV (Fig. 7). Measurements taken immediately after cleaving the sample (curve *1*) exhibit a sharp (resolution limited) Fermi edge and significant spectral weight in the region 1–2 eV below E_F. Heating the sample to 300 K radically changes the spectrum (curve *2*): intensity is reduced both at the Fermi level and in the region 1–2 eV below it. Also, the peak of the valence bands shifts from 3.5 to 4.5 eV and a satellite appears at 9 eV below E_F. Subsequent cooling of the sample down to 20 K (curve *3*) shows the changes to be irreversible. Figure 8 compares the regions in the immediate vicinity of E_F for the high temperature superconductor $Pb_2Sr_2Y_{0.5}Ca_{0.5}Cu_{2.25}Ag_{0.75}O_8$ (curve *1*), ordinary metal (curve *2*), and the semiconductor $Pb_2Sr_2YCa_2Cu_3O_8$ (curve *3*) (data from Ref. 10). These measurements clearly confirm the existence of a sharp Fermi edge in high-T_c superconductors just as in ordinary metals and thereby support the validity of the Fermi-liquid description of charge carriers.

Let us now discuss the shift of HTSC valence bands

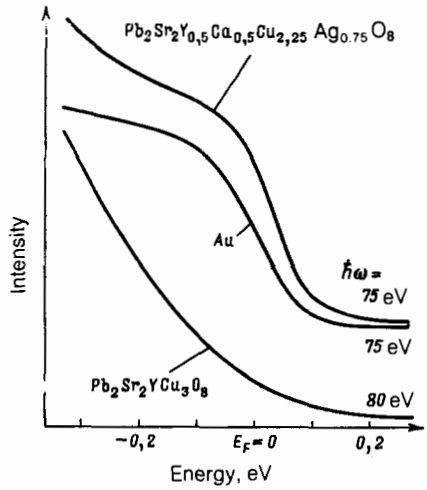

FIG. 8. Photoemission spectra measured at 75–80 eV photon energy[10] near the Fermi level of the $Pb_2Sr_2YCu_2O_8$ semiconductor, $Pb_2Sr_2Ca_{0.5}Cu_{2.25}Ag_{0.75}O_8$ high-temperature superconductor, and thick Au film.

towards higher binding energies with respect to the theoretically calculated density of states. As before, this shift is probably due to evolution of oxygen from the sample surface (Fig. 7). A comparison of measurements on freshly cleaved samples[9] with theoretical photoemission spectra computed in the band structure framework shows only a small remaining shift of 0.5 eV (Fig. 9). Thus, the theoretical spectral lineshape is in good agreement with experiment.

Furthermore, theoretical spectra exhibit a nearly one-

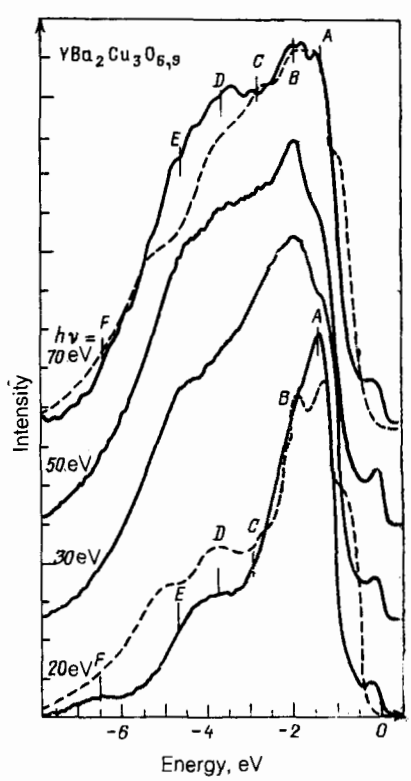

FIG. 9. Comparison of calculated and measured photoemission spectra. Solid lines are measured spectra[9] with the secondary electron background subtracted. Dashed lines are calculated spectra[11] shifted by 0.5 eV towards higher binding energies.

to-one correspondence with features labeled with letters A–F (Fig. 9) which indicates that calculations of the density of states accurately estimate the hybridization of copper and oxygen orbitals. The remaining discrepancies–0.5 eV shift and the excessively sharp jump at the Fermi edge–are either the result of surface effects or real dynamical electron-electron interaction processes.

Let us turn now to one of the basic questions of the satellite structure in HTSC photoemission spectra. The significance of this structure is due to the following. Most of the models proceeding from the Hubbard Hamiltonian assume the electronic states of copper to be localized, resulting in a nearly atomic configuration of the Cu^{2+}–$3d^9$ ion. This completely contradicts the band structure approach, which assumes strong hybridization of copper d- and oxygen p-orbitals. The existence of satellites in photoemission spectra can be taken as evidence of copper electron localization. And indeed, early experimental studies did observe satellite structure 9–12 eV below the main valence band (Fig. 10, reproduced from Ref. 12). Electron localization at copper sites provides a trivial explanation: ionization of the Cu^{2+} state produces the $3d^9 \to 3d^8$ configuration, i.e. two holes appear in the d-shell of copper and these holes repel each other with energy U. The ionization energy in this scenario is $|\varepsilon_d - U|$, where ε_d is the single-electron level of the d-electron. Consequently the satellite is nothing but the direct photoemission signature of the Cu^{3+}. A possible explanation for the two satellite peaks can invoke the formation of a two-hole state of the O^{2-} ion during photoemission.

In fact, screening effects should certainly weaken the satellite intensity in comparison to the main valence band. In other words, screening charge can leak into the d-shell simultaneously with the $3d^9 \to 3d^8$ ionization. Roughly speaking, this should produce such final copper states as $|d^8 d^* >$ or $|d^8 s^* >$, where d^* and s^* are the screening charges in d- and s-shells respectively. These screening effects and the hybridization of d-states with oxygen orbitals should determine the relative intensities of the satellite and valence band peaks. In the band structure limit of strong hybridization, the photohole created in the d-shell is always screened by charge leaking in from the oxygen sites via the covalent bond and the satellite peak should disappear.

This picture of satellite behavior should be complemented by yet another mechanism for the appearance of satellites. Suppose that the photon energy is near the 3p–3d excitation threshold of copper ($\hbar\omega = 74$ eV). Then electron excitation from the valence band will be accompanied by electron transitions from the occupied atomic 3p-level into

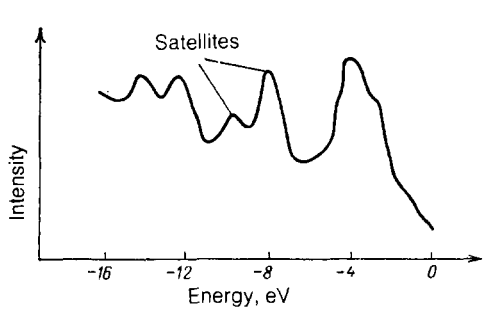

FIG. 10. Photoemission spectrum of $La_{2-x}Sr_xCuO_4$[12] with well-defined satellite structure in the 8–12 eV region.

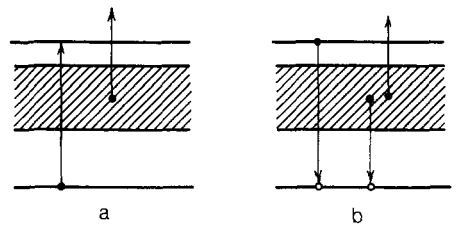

FIG. 11. Schematic diagram of Auger processes: a–photoemission is accompanied by excitation of a core electron into the conduction band; b–two available hole recombination channels: capture of the excited electron or capture of a valence electron accompanied by simultaneous emission of another.

the conduction band (Fig. 11, a). The resulting hole, localized at the 3p-level, will recombine via one of two channels (Fig. 11, b). The first of these channels is direct recombination, with the excited electrons dropping down directly into the 3p-level. The second channel consists of an Auger process, with the hole recombining with one of the d-band electrons while a second d-electron is simultaneously emitted into a higher-lying band. This last channel creates a two-hole state in the d-band that is different from the ionic Cu^{3+} state. Consequently, the band structure description also can accommodate one satellite in HTSC spectra at frequencies near the 3p–3d threshold. (Note that such a satellite is indeed observed in pure copper with a completely filled d-band[13]).

But what about the most up-to-date experiments on freshly cleaved samples at low temperatures?[9] First, these measurements show no satellite whatsoever at 9 eV until the sample is heated, at which point the satellite reappears (Fig. 7). Second, no satellite structure in the 9 eV region is observed in freshly cleaved samples with oxygen content ~ 6, i.e. in the antiferromagnetic phase of HTSC.[9] This leads one to conclude that the 9 eV satellite is not intrinsic to either the metallic or the antiferromagnetic phase, but rather is a purely surface effect or else an artifact of surface contamination. Third, Arco and co-workers demonstrated[8] that the small satellite in the 12 eV region resonates only near the 3p–3d threshold (Fig. 12). As discussed above, this effect does not contradict the band structure description, being a signature of the formation of a two-hole copper state via an Auger process, rather than a photoemission process.

The last point which should be addressed in connection with the satellite structure is the possibility of 12 eV satellite observation far from the 3p–3d threshold. In this regard we should recall the well-known photoemission effect in Ni,[14] where sd-hybrid bands reach the Fermi surface and the electron configuration roughly corresponds to $3d^9 4s^1$. In that system photoemission can involve two processes: $3d^9 4s^1 \to 3d^8{*}d^*4s^1$, i.e. the photohole is screened by d-electrons, contributing to the valence band signal in the spectrum, and $3d^9 4s^1 \to 3d^9 4s^1 s^*$, i.e. s-screening which produces a satellite near 7 eV that does not coincide with the energy of the $3d^8$ state of the Ni ion. A theoretical investigation of this effect was attempted by a number of authors,[15] who attributed it to the nontrivial behavior of the spectral function of the additional hole. It was shown that this function is

$$A_{ki}(\omega) = \frac{1}{\pi} \frac{\operatorname{Im} \Sigma_{ki}(\omega)}{(\omega - E_{ki} - \operatorname{Re} \Sigma_{ki}(\omega))^2 + (\operatorname{Im} \Sigma_{ki}(\omega))^2}, \quad (26)$$

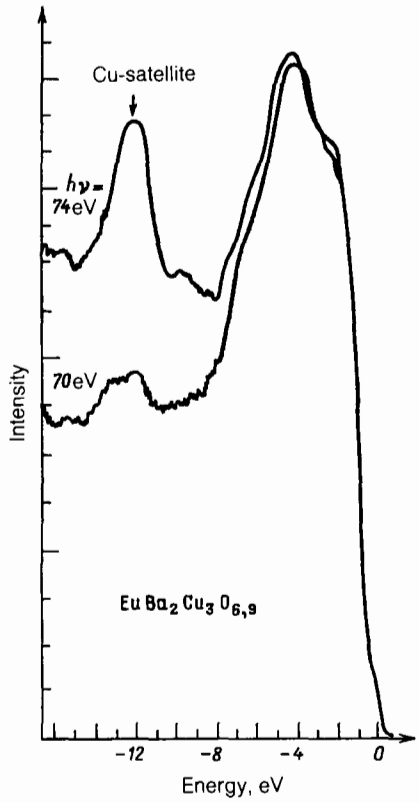

FIG. 12. Photoemission spectra of $EuBa_2Cu_3O_{6.8}$.[8] The satellite in the 12 eV region is resonantly enhanced at $\hbar\omega = 74$ eV.

where E_{ki} is the electron excitation spectrum in the band approximation; $\Sigma_{ki}(\omega)$ is the self-energy component of electron energy arising from dynamical electron-electron interactions. The spectral function (26) can exhibit resonances in two regions. The band spectrum produces a resonance near $\omega \approx E_{ki}$, while a second resonance can arise from singularities in the $\Sigma_{ki}(\omega)$ dependence. In the scattering matrix approximation for electrons, an approximate expression for $\Sigma_{ki}(\omega)$ can be written as follows:

$$\Sigma(\omega) \approx \frac{U}{1 + Ug_2(\omega)}, \tag{27}$$

where U is the electron-electron repulsion at the same site; $g_2(\omega)$ is the two-hole Green's function. As long as U is not too small, the denominator of (27) can go to zero at frequencies lying outside the single-particle energy range. This singularity in the self-energy corresponds to the quasi-bound state of two holes and can produce a satellite in the photoemission spectrum. Apparently this is the origin of the weak satellite in the $\hbar\omega \approx 12$ eV region that is observed far from the 3p–3d threshold in high-temperature superconductors.

Let us conclude this section by listing the main results that can be deduced from the above data. First of all, the existence of a Fermi edge in HTSC that is as sharp as the Fermi edge in ordinary metals conclusively proves that HTSC electronic structure behaves as a Fermi liquid. Further, the 2 eV shift of photoemission spectra with respect to theoretical predictions observed in early experiments have been reduced to 0.5 eV by more accurate measurements, while the strong 9 eV satellite is clearly absent from both metallic and antiferromagnetic phases. As for the weak satellite in the 12 eV region that resonates near the 3p–3d threshold, this is insufficient evidence for claiming that the 3d-states of copper are localized and that the band structure description is therefore inadequate. Certainly, the remaining discrepancies–0.5 eV shift in the binding energy, smaller than expected density of states at the Fermi energy, and the weak satellite at $\hbar\omega \approx 12$ eV–all indicate that dynamical exchange correlation effects play a substantial role in the electronic structure of HTSC. The one remaining question concerns the best method of quantitatively describing these effects. In this connection, we should mention the work of Costa-Quintana and co-workers,[16] who attempted to calculate the changes in the band spectrum due to dynamical electron-electron interaction neglected in the density functional formalism. They employed a fairly simple model approach that ignored, among other things, the dispersion of the Coulomb interaction matrix element, so the quantitative results are somewhat suspect. What is more important, however, is the demonstration that all the aforesaid discrepancies between photoemission spectra and band structure calculations can be reconciled relatively easily by taking dynamical correlations into account.

6. ANGLE-RESOLVED PHOTOEMISSION EXPERIMENTS

Generally speaking, angle-resolved photoemission measurements should suffice to determine the band structure of layered compounds. The large number of bands in HTSC causes several problems, however. First, the energy resolution of the spectrometer is finite. Currently, typical experimental resolution in the ultraviolet falls in the 0.1–0.2 eV range and therefore the peaks corresponding to single bands are difficult to distinguish among many. It is more feasible to estimate the intensity contributions of whole groups of bands and then attempt to deduce correlations between observed peaks and calculated band structure. Keep in mind, however, that several research groups have improved their experimental resolution by almost an order of magnitude, down to 0.02 eV.

There are other problems. They include, for example, effects caused by the finite lifetimes of quasiparticle states. The spectral linewidth produced by a given band is a function not only of instrumental resolution, but also of the lifetimes of the photohole created in the filled band and the excited photoelectron emitted into a higher-lying band. The inverse lifetime of the photohole is given by the imaginary part of the self-energy and behaves like $\sim\omega^2$ in Fermi liquid theory, where $\hbar\omega$ is the energy measured referred to the Fermi level. Consequently, the linewidths produced by this effect are minimal for electrons emitted from the Fermi surface. Another contribution to the linewidth is due to the finite lifetime of the excited electron propagating through the crystal and into the detector. This effect will set a lower bound on the linewidth, even for electrons emitted from E_F and detected with infinite instrumental resolution.

Angle-resolved photoemission measurements have been carried out both on 1:2:3 compounds and bismuth cuprates. The spectra of $Bi_2Sr_2CaCu_2O_8$ compounds along the ΓX axis in the Brillouin zone at $\hbar\omega = 18$ eV are shown in Fig. 13.[17] These spectra contain several features that are marked with arrows. The main result that can be deduced by assuming that each feature corresponds to a band is that the bands appear to have no dispersion in the plane, which contradicts the band structure description, as discussed earlier.

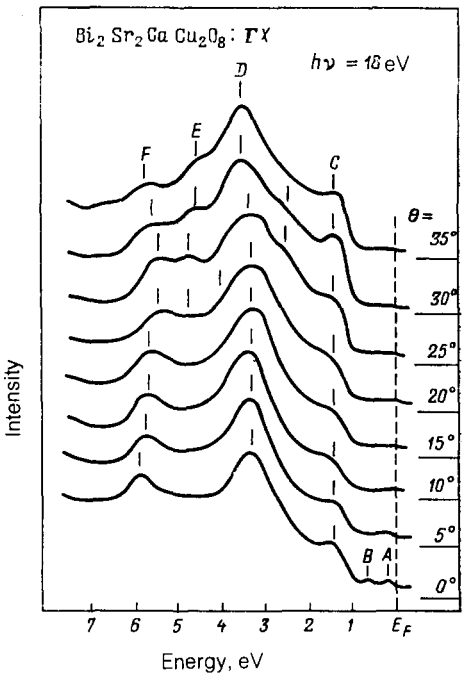

FIG. 13. Angle-resolved photoemission spectra of $Bi_2Sr_2CaCu_2O_6$ measured at $\hbar\omega = 18$ eV for the ΓX direction in the Brillouin zone. Polar angle referred to the surface normal is indicated on each spectrum.

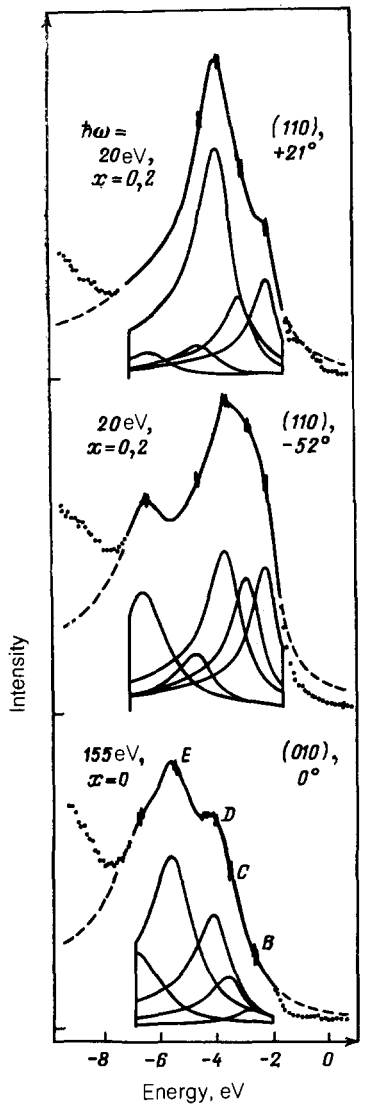

FIG. 14. Typical valence band spectra of $(Bi_{1-x}Pb_x)Sr_2CaCu_2O_8$ and calculated Doniach–Sunich fitting curves.[18]

On the other hand, the large angle-dependent shifts in feature structure indicate, if nothing else, that the features are probably due to entire groups of bands and hence interpretation of spectra in terms of band structure is rather difficult. The most rigorous analysis of spectral lineshape in angle-resolved photoemission was attempted by Böttner and co-workers.[18] They assumed that the spectrum can be expressed as a sum of lines corresponding to interband transitions. The lineshapes were written in terms of Doniach-Sunich functions (see review,[1] for example) that correspond to asymmetric Lorentz distributions (Fig. 14). The linewidth was assumed to depend on energy, while the asymmetry parameter took into account screening of the hole by low-energy excitations and was assumed the same for all transitions. Thus, by modeling changes in the photoemission spectrum as a function of electron energy and emission angle, Böttner and co-workers constructed a band spectrum pictured in Fig. 15. This spectrum indicates significant dispersion in the a,b plane, in reasonable agreement with theoretical calculations.

The situation is equally complicated in the immediate vicinity of the Fermi energy. The large number of bands lying within 1 eV of E_F (5–6 bands in 1:2:3 compounds) makes it practically impossible to distinguish their individual contributions with instrumental resolution of the order of 0.1–0.2 eV. On the other hand, by identifying the features in photoelectron spectrum with individual bands one can deduce the dispersion laws near E_F. This procedure was carefully implemented by Sakisaka and coworkers.[19] One of the sets of spectra measured along the Γ–X–M–Γ directions of the Brillouin zone in 1:2:3 compounds is shown in Fig. 16. The spectra contain a good number of peaks, troughs, shoulders, etc. Some of the main features are marked with arrows. The band structure near E_F reconstructed from these features is shown in Fig. 17. It is in adequate agreement with calculations.[20] The main result here is the existence of a dispersive branch that crosses the Fermi level, which supports the validity of the Fermi liquid description of high-temperature superconductors. Despite this good agreement of experiment with single-particle theory, we should note that the spectra of Fig. 16 do not allow for a convincing one-to-one identification of the weak features with individual bands. Because of broadening, the features cannot be considered strong evidence of the correctness of calculated band spectra.

At this point it appears helpful to discuss briefly some recently published experimental results of angle-resolved photoemission from $Bi_2Sr_2CaCu_2O_8$ single crystals that have engendered much debate. The photoemission spectra measured for a number of angles along the ΓY direction in Brillouin zone using 22 eV photons are shown in Fig. 18. Measured electron dispersion curves (points) are plotted in the inset together with calculated results.[20] In the inset we find that the measured and calculated dispersions $E(\mathbf{k})$ agree at the point they cross the Fermi level. This indicates that the experimentally determined and calculated Fermi surfaces also agree. Moreover, the experimental $E(\mathbf{k})$ curves

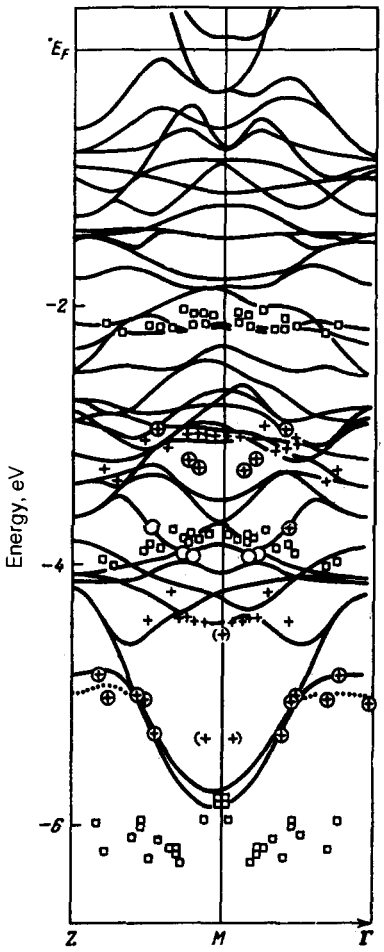

FIG. 15. Solid lines represent the calculated band structure of $Bi_2Sr_2CaCu_2O_8$. Experimental points are shifted by 0.3 eV towards lower binding energies with respect to the calculation.

exhibit significant dispersion, while the effective electron mass calculated from the dispersion curves is larger than that obtained in band structure calculations by a factor of two. This could point to the existence of sufficiently strong dynamical electron correlations or electron-phonon interaction that renormalize the electron mass. This phenomenon can be adequately treated within the framework of standard Fermi liquid theory.

A radically different interpretation of the results shown in Fig. 18 (but not the inset!) was proposed by P. Anderson, the author of the resonating valence bond (RVB) theory (see, for example, his lecture in collection[22]). Anderson considers these data to be a clear experimental confirmation of the RVB theory of HTSC. On what grounds? First of all, he points to the sharp change in the spectrum near the Fermi edge, indicating little spectral broadening on the wavevector scale of $\Delta k \sim 0.1 k_F$, where k_F is the Fermi wavevector. He believes that estimates based on resistance measurements indicate that the electron mean free path in these compounds, limited by inelastic scattering from charged impurities, should be of the order of interelectron spacing $l \sim 1/k_F$, such that $\Delta k \sim k_F$. Hence the sharp change in photoemission spectra at $k \sim k_F$ is not due to the electron Fermi surface, but rather to the "quasi-Fermi" surface of uncharged RVB theory quasiparticles–spinons, which naturally do not interact with charged impurities. In these spectra Anderson also

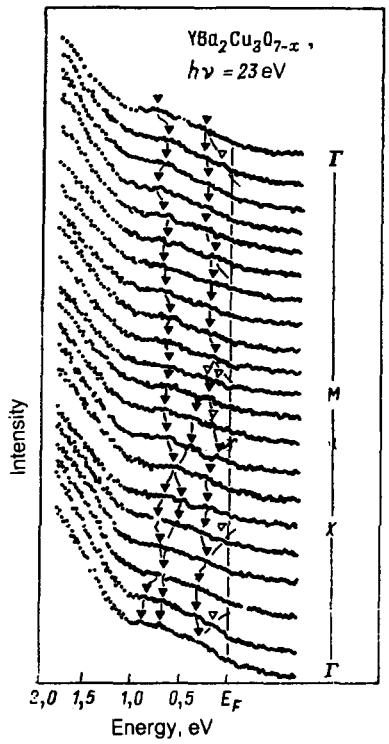

FIG. 16. Angle-resolved photoemission spectra of $YBa_2Cu_3O_{7-x}$ near the Fermi level, measured with $\hbar\omega = 23$ eV and $\theta_i = 60°$ along the Γ-X-M-Γ directions of the Brillouin zone.[19]

points to the rather large background away from the Fermi surface, which he attributes to the properties of the RVB state. It is no simple matter to discuss the validity of Anderson's assertions, especially since little detail is available in his published work. However, we believe a comparison of photoemission curves near the Fermi edges of a normal metal (platinum) and the $Bi_2Sr_2CaCu_2O_8$ compound to be ex-

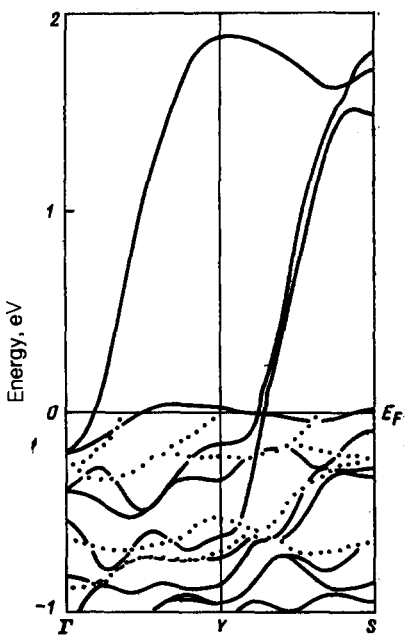

FIG. 17. Comparison of experimental and theoretical band structure of $YBa_2Cu_3O_{7-x}$ near the Fermi level. Circles represent experimental results of Ref. 19; solid lines are the calculation of Ref. 20.

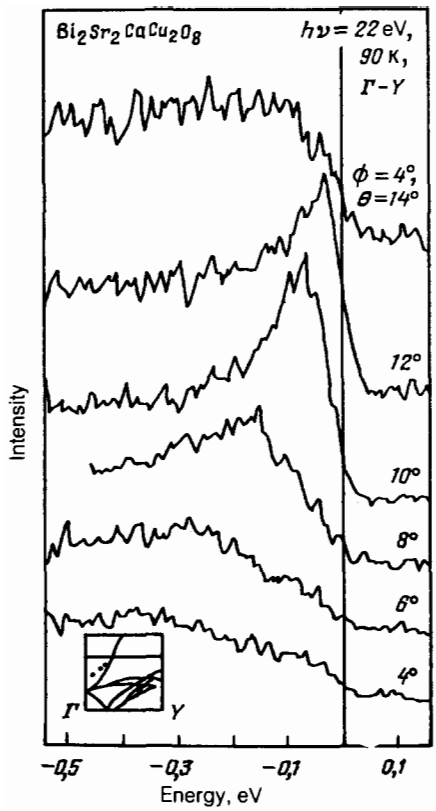

FIG. 18. Angle-resolved photoemission spectra for several angles along the ΓY direction of the Brillouin zone measured with $\hbar\omega = 22$ eV.[21] Inset compares the measured dispersion (points) with the calculation of Ref. 20.

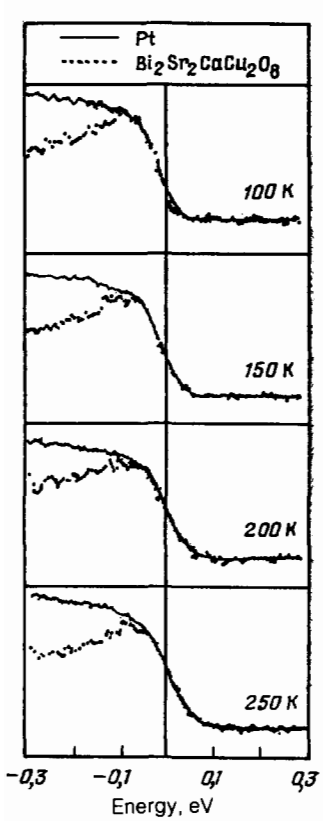

FIG. 19. Comparison of Fermi edge in platinum and in $Bi_2Sr_2CaCu_2O_8$ at several temperature values between 100 K and 250 K.[21] The spectra are normalized along the ordinate axis but not shifted horizontally.

tremely instructive in this regard (see Fig. 19, the data are also from Ref. 21). We find in Fig. 19 that the behavior of these curves near the Fermi edge is quite identical. As for the background far from the Fermi energy, it is even higher in platinum. Granted, the Pt curves also contain a distinct spectrum of spin fluctuations, but we believe the claims of the existence of RVB-states in this metal to be premature.

In conclusion, there is no direct experimental evidence for the dispersion laws derived within the single-electron band structure framework. Here the fundamental problem lies in the large number of bands and the finite instrumental resolution, as well as the finite lifetime of electronic states. On the other hand, we should note that state-of-the art instrumental resolution is now pushing 0.01 eV. This should be sufficient to distinguish individual bands, at least near the Fermi level. Another caveat is necessary at this point. The absence of a peak in the photoemission spectrum need not indicate the absence of a band in the band structure. Instead, the cause could be a weak matrix element or the absence of an allowed band for the excited final state. Accordingly, measurements should be carried out at a series of photon energies to avoid this problem. There is every expectation that our understanding of this region will improve in the very near future.

Recent improvements in instrumental resolution down to 0.01 eV have made it possible to observe the changes in the photoemission spectrum associated with the transition to a superconducting state. We know that this transition produces a gap in the excitation spectrum. The density of states near this gap behaves as follows:

$$N(E) = \frac{E}{(E^2 - \Delta^2)^{1/2}} \tag{28}$$

with $E > \Delta$. Hence the superconducting transition should manifest itself by a singularity near E_F in the photoemission spectrum. The finite instrumental energy resolution together with dynamical electron-electron interaction effects will produce broadening, but some signature of the singularity should remain. Figure 20 compares the normal Fermi step at 300 K with a superconducting density of states, where both functions are convolved with a Gaussian to simulate instrumental resolution $\Delta E = 0.03$ eV. Data reported in Refs. 23,

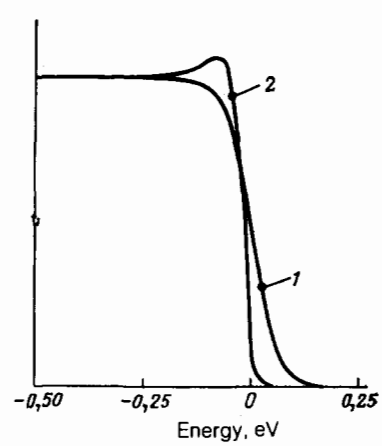

FIG. 20. Fermi–Dirac function at $T = 300$ K (curve 1) and the superconducting density of states at $\Delta = 30$ meV (curve 2). Both functions are convolved with a Gaussian to model instrumental resolution of $\Delta E = 30$ meV.

24 are in excellent agreement with Fig. 20. Measurements on $YBa_2Cu_3O_7$[21] and $Bi_2Sr_2CaCu_3O_8$[22] compounds not only reveal the appearance of an energy gap during the superconducting transition, but also make it possible to estimate the size of the gap. The values obtained are quite large, leading to the ratio $2\Delta/kT_c \approx 6$–8. Olson and co-workers[25] employed photoemission spectroscopy to establish the angular dependence of the energy gap in the a, b plane and found it to exhibit no significant anisotropy.

7. CONCLUSION

This review did not attempt to discuss the full scope of photoemission experiments on HTSC materials. Instead we focused on the agreement (or lack thereof) between experimental photoemission data and the standard description of HTSC materials within the band structure framework. This comparison is quite significant, as it lays the groundwork for theoretical investigations of HTSC systems. What is our outlook on this question? It is abundantly clear that early photoemission measurements, performed on imperfect samples without taking into account the rapid degradation of surface properties, etc., have led to unwarranted conclusions that band structure methods were completely inadequate for describing electrons in HTSC. As this review indicates, new experimental results, obtained on improved samples with greatly improved instrumental resolution, can be described reasonably well precisely by the usual band structure picture. Granted, the data also reveal some consistent deviations from the predictions of band structure calculations, pointing to the important role of dynamical electron correlations. Unfortunately, the precision of current experimental measurements and, more significantly, the insufficiently consistent theoretical models that incorporate exchange and correlation effects are quite inadequate for a quantitative understanding of the correlation effects. This is especially true of the electronic states near the Fermi level. Much theoretical and experimental research remains to be carried out before we can fully understand the electronic structure of high-temperature superconductors.

The authors express their deep gratitude to V. L. Ginzburg, D. A. Kirzhnits, and the participants in their seminars for fruitful discussions of the materials included in this review.

[1]M. Cardona and L. Ley (editors), *Photoemission in Solids*, Springer-Verlag, Berlin, Heidelberg, New York, Vol 1: General Principles, 1978; Vol 2: Case Studies, 1979.
[2]S. Lundqvist and N. H. March (editors), *Theory of Inhomogeneous Electron Gas*, Oxford University Press, Oxford, 1983 [Russ. transl., D. A. Kirzhnits and E. G. Maksimov (editors), Mir, M., 1983].
[3]G. Wendin, J. de Phys. C **9**, 1157 (1987).
[4]F. C. Zang and J. M. Rice, Phys. Rev. B **37**, 3759 (1988).
[5]C. M. Varma, S. Schmitt-Rink, and E. Abrahams, Solid State Commun. **62**, 681 (1987).
[6]P. W. Anderson, Science **235**, 1196 (1987); P. W. Anderson, G. Baskaran, Z. Zou, and T. Hsu, Phys. Rev. Lett. **58**, 2790 (1987).
[7]M. Onellion, Ming Tang, Y. Chang, G. Margaritondo, J. M. Tarascon, P. A. Morris, W. A. Bonner, and N. G. Stoffel, Phys. Rev. B **38**, 881 (1988).
[8]A. J. Arco, R. S. List, Z. Fisk, C. -W. Cheong, J. D. Thompson, J. A. O'Rourke, C. G. Olson, A. B. Yang, T. W. Pi, J. E. Schirber, and N. D. Shinn, J. Mag. Mag. Mater. **75**, L1 (1988); R. S. List, A. J. Arco, Z. Fisk, J. D. Thompson, C. B. Pierce, D. E. Paterson, R. J. Bartlett, N. D. Shinn, J. E. Schirber, B. W. Veal, A. P. Paulikas, and J. C. Campuzano, Phys. Rev. B **38**, 11966 (1988).
[9]A. J. Arco, R. S. List, R. J. Bartlett, C. -W. Cheong, Z. Fisk, J. D. Thompson, C. G. Olson, A. -B. Yang, R. Lie, C. Gu, B. W. Veal, J. Z. Lie, A. P. Paulikas, K. Vandervoort, H. Claus, J. S. Campuzano, J. E. Schirber, and N. D. Shinn, Phys. Rev. B **40**, 2268 (1989); Physica Ser. C **159**, 439 (1989).
[10]Y. How, Y. Chang, M. Onellion, and G. Margaritondo, Solid State Commun. **71**, 415 (1989).
[11]J. Redinger, A. J. Freeman, J. Yu, and S. Massida, Phys. Lett. A **124**, 469 (1987).
[12]P. Thiry, G. Rossi, Y. Petroff, A. Revcolvchi, and J. Jegodez, Europhys. Lett. **5**, 55 (1988).
[13]M. R. Thuler, R. L. Bendow, and Z. Hurych, Phys. Rev. B **269**, 669 (1982).
[14]C. Guillot, Y. Ballu, J. Paigne, J. Lecante, K. P. Jain, P. Thiry, R. Pinchaux, Y. Petroff, and L. M. Falicov, Phys. Rev. Lett. **39**, 1632 (1977); S. Hüfner and G. K. Wertheim, Phys. Lett. A **51**, 299 (1978).
[15]D. R. Penn, Phys. Rev. Lett. **42**, 921 (1979); L. A. Feldkamp and L. C. Davis, Phys. Rev. Lett. **39**, 1632 (1977); A. Liebsch, Phys. Rev. Lett. **43**, 1431 (1979).
[16]J. Costa-Quintana, F. Lopez-Aguilar, and S. Balle, Phys. Rev. B **39**, 9675 (1989).
[17]T. Takahashi, H. Matsuyama, H. Katayama-Yoshida, Y. Okabe, S. Hosoya, K. Seki, H. Fujimoto, M. Sato, and H. Inokuchi, Phys. Rev. B **39**, 6636 (1989).
[18]R. Böttner, N. Schroeder, E. Dietz, U. Gerhardt, W. Assmus, and J. Kowalewski, Phys. Rev. B (to be published) (1990).
[19]Y. Sakisaka, T. Kometa, T. Maruyama, M. Onci, H. Kato, Y. Ainra, H. Yanashima, T. Terashima, Y. Bando, K. Jijima, K. Katamoto, and K. Hirata, Phys. Rev. B **39**, 9080 (1989).
[20]J. Yu, S. Massida, A. J. Freeman, and D. D. Koelling, Phys. Lett. A **122**, 203 (1987).
[21]C. G. Olson, R. Liu, D. W. Lynch, B. W. Veal, Y. C. Chang, P. Z. Jiang, J. Z. Liu, A. P. Paulikas, A. J. Arko, and R. S. List, Physica Ser. C **162–164**, 1697 (1989).
[22]P. W. Anderson, *Lecture Notes on Current Trends in Condensed Matter Physics, Particle Physics, and Cosmology*, Katmandu, June 1989.
[23]Y. Chang, Ming Tang, R. Zanoni, M. Onellion, R. Joynt, D. L. Huber, G. Margaritondo, P. A. Morris, W. A. Bonner, J. M. Tarascon, and N. G. Stoffel, Phys. Rev. B **39**, 4740 (1989).
[24]J. M. Imer, F. Pathney, B. Darbell, W. D. Schreider, V. Boer, Y. Petroff, and A. Zettl, Phys. Rev. Lett. **62**, 336 (1989).
[25]C. G. Olson, R. Lin, A. B. Yang, and D. W. Lunch, Science **245**, 731 (1989).
[26]G. A. Burdick, Phys. Rev. **129**, 138 (1963).
[27]P. Thiry, D. Chandesris, J. Lecante, C. Guillot, R. Pinchaux, and Y. Petroff, Phys. Rev. lett. **43**, 82 (1979).

Translated by A. Zaslavsky